The International Journal of Advanced Manufacturing Technology (2019) 103:2121–2132
https://doi.org/10.1007/s00170-019-03631-3

ORIGINAL ARTICLE

Towards aging in a multipass friction stir–processed AA2024

K. N. Kalashnikov[1] · S. Yu. Tarasov[1] · A. V. Chumaevskii[1] · S. V. Fortuna[1] · A. A. Eliseev[1] · A. N. Ivanov[1]

Received: 27 December 2018 / Accepted: 22 March 2019 / Published online: 17 April 2019

Abstract
Multipass friction stir processing was applied to AA2024 8-mm-thick samples with the goal of studying the microstructural evolution of the metal processed. Up to three parallel FSP tracks with an overlap of 0.375 between the neighboring ones have been obtained on the samples and then characterized for microstructure and mechanical strength. Clear macroscopic zones between the tracks have been observed. The specificity of microstructural evolution in the fine crystalline part of the thermo-mechanically affected zone formed close to the stirring zone is its over-aging due to less intensive strain dissolution of precipitates as compared with that of the stirring zone. The minimum hardness zone is formed there while higher hardness is observed in the less deformed part of the zone due to S(S′) (Al_2CuMg) precipitates. The thermo-mechanically affected zone formation was considered from the viewpoint of tribology when the stirring zone metal flow slides over the thermo-mechanically affected zone metal and deforms it.

Keywords Multipass friction stir processing · Aluminum alloy · Aging · Sliding-induced zones

1 Introduction

The multipass friction stir processing (MP-FSP) might be referred to as a severe plastic deformation (SPD) process aimed at improving mechanical characteristics of the processed metal. There are several SPD methods, such as equal channel angular pressing and rolling, that can be used to obtain bulk ultrafine-grained materials. On the other hand, there are SPD methods like burnishing used only to improve mechanical characteristics of surface layers. With friction stir processing and using a specially designed tool, it is possible to obtain a thin subsurface fine-grained layer or even a bulk nanostructured material. It was shown by Gandra et al. [1] that one of the main issues in the multipass friction stir processing is the effect of overlapping, which is very important for the metal strength, surface morphology, and hardness distribution uniformity. It is obvious that metal in the overlap zone is subjected to re-heating and re-stirring resulting from forming the next track, and therefore, some additional structural changes may occur there. Such a situation is often met when directed energy fusion deposition processes are applied, for example, plasma torch multipass deposition results in forming quenched martensite subzones in the re-heated zone which is a detrimental factor for abrasive wear [2]. The plasticized metal flow in MP-FSP is not melted and therefore residual stresses in the heat-affected zone are not commonly high; however, it may depend on the type of alloy. A heat-hardenable alloy like AA2024 may give extra precipitation hardening in this zone after friction stir welding.

Similar to that of friction stir–welded metal, the overlapping zone between two successive friction stir–processed (FSPed) tracks thus must include two zones known as heat-affected (HAZ) and thermo-mechanically affected zones (TMAZ). The specificity of these zones is that both of them have been formed in a previously FSPed fine-grained metal, which is susceptible to superplastic flow and thus shows less mechanical resistance to FSP. For example, mechanical resistance to FSP reduced from 1000 to 300 kg in crossing the previously made FSP track on AA 2024 (Fig. 1). Such a phenomenon has also been discovered by Brown and Reynolds who noticed that the travel force is reduced when welding on the previously welded metal [4].

Therefore, a rotating FSP tool may draw more metal into the flow and thus form a re-stirred zone 2 and wide TMAZ. In addition, the first stir zone grains which are not involved into this flow may experience re-heating and finally grow or extra

✉ S. Yu. Tarasov
tsy@ispms.ru

[1] Institute of Strength Physics and Materials Science SB RAS, Tomsk, Russian Federation

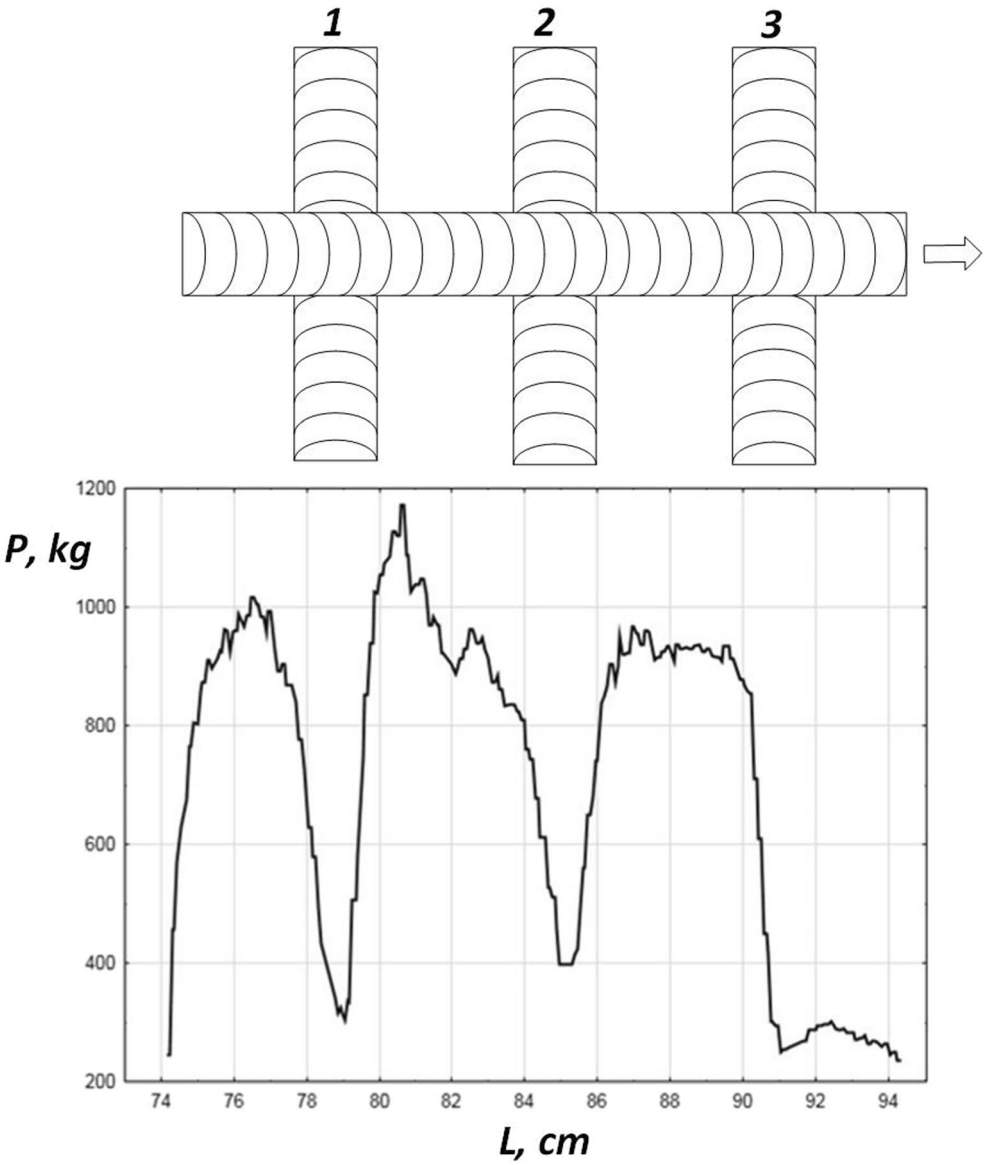

Fig. 1 The mechanical resistance of processed metal to the FSP tool travel [3]

age. It is obvious that the overlapping zone in wrought aluminum alloys would be therefore less structurally distinguished as compared with those formed in stirred or re-stirred zone on the heat-hardenable alloy.

The microstructure and microhardness number distribution on AA2024 friction stir-welded joints shows that the precipitation kinetics is depended on the strain achieved in different zones. In particular, it was by shown by Genevois et al. [5] that over-aged microstructure of TMAZ was responsible for the formation of microhardness minimum zones. However, the microstructures shown look like those of additionally age-hardened HAZ zones. In our opinion, the TMAZ should be considered as composed of two zones; one of them consisted of very fine grains (TMAZ I) and another one represented by coarse but plastically deformed grains (TMAZ II).

The less extensive grain refinement zone with voids was detected by Abraham [6] in the overlap zone between two successively made MP-FSP tracks. It is feasible that this zone experienced re-heating and grain growth.

It is undisputable that structural inhomogeneity resulting from the MP-FSP metal may have its negative effect on the metal strength and fatigue characteristics.

The objective of this paper is to characterize and compare samples obtained using one-pass, two-pass, and three-pass MP-FSP on 2024 alloy.

2 Materials and methods

A heat-hardenable aluminum alloy 2024 of the composition shown in Table 1 was utilized for experimental

Table 1 Chemical composition of 2024 aluminum alloy, wt.%

Fe	Si	Mn	Cr	Ti	Al	Cu	Mg	Zn	Impurities	–
0.5	0.5	0.3–0.9	0.1	0.15	90.9–94.7	3.8–4.9	1.2–1.8	0.25	Each 0.05; total 0.15	Ti + Zr < 0.2

MP-FSP using a laboratory FSW machine (Fig. 1a—general view, Fig. 2b—welding unit). The alloy workpiece was an 8-mm-thick sheet with parallel MP-FSP tracks and a 5-mm penetration made using a standard FSW tool made of AISI H13 steel. The overlap was determined according to formula OR = 1 − (*L*/*d*) = 0.375, where *L* = 5 mm is the distance between the successive parallel track centerlines and *d* = 8 mm is the pin's diameter [6]. The FSP process parameters were as follows: plunging force 3600 kg, speed 90 mm/min, rotation rate 450 RPM. Total three series of samples such as one-pass, two-pass and three-pass were made for comparison reason (Fig. 2c). Specimens for investigations were cut of the samples as shown in Fig. 2c.

Structural evolution of the MP-FSP metal was examined using the optical and scanning laser microscope Olympus OLS4100 on polished specimens etched using the Keller reagent. Microstructural characterization of the samples was carried out using a TEM instrument JEM-2100 (JEOL Ltd., Japan). Thin foils for TEM studies have been prepared using an EM-09100IS (JEOL Ltd., Japan) sample preparation system. Mechanical characterization of the samples was performed by compression and tension at ambient temperatures using a Testsystems 110M-10 tensile machine. Microhardness tests were carried out using a Vickers TTX-THT Nano Hardness Tester (CSM-Instruments).

3 Results

3.1 Macrostructure

3.1.1 Single-Pass FSP

A single-pass FSP track forms a stirring zone as well as a thermo-mechanically affected zone (TMAZ) and a heat-affected zone (HAZ) in AA2024 similar to those obtained in FSW (Fig. 3a). The base metal structure (Fig. 3a) is composed of coarse grains elongated with respect to hot-rolling direction. The microhardness profile shows the low hardness of the stirring zone (SZ1), even lower microhardness of the thermo-mechanically affected zones both on the advancing and retreating sides (Fig. 4b) and high hardness of the heat-affected zones formed due to extra aging. The stirring zone structure is represented by equiaxed recrystallized grains smaller than those of the base metal by a factor of 50 (Fig. 4a, b). The TMAZ zone structure on the advancing side is composed of elongated grains which form a sharp and clear boundary with the stirring zone (Fig. 5b) while the retreating side TMAZ grains become oriented with respect to the stirring zone metal flow (Fig. 5a) and thus result in a wide and diffuse boundary with the stirring zone.

Fig. 2 Laboratory FSW machine (**a**) FSW welding unit (**b**) and schematics of the MP-FSP (**c**). 1—spindle; 2—FSW tool; 3—workpiece

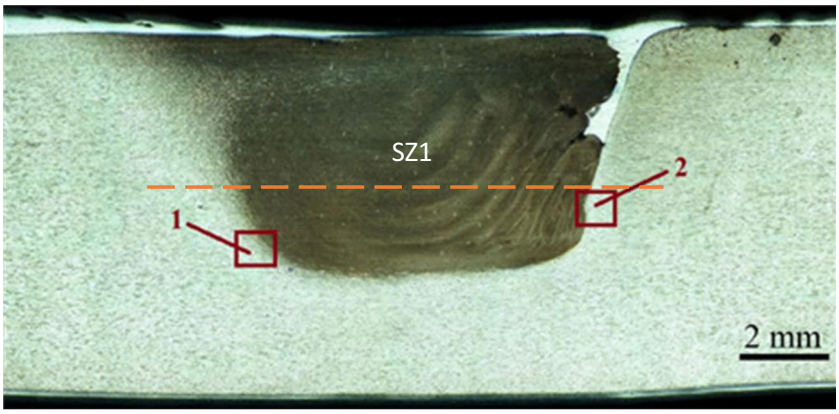

a)

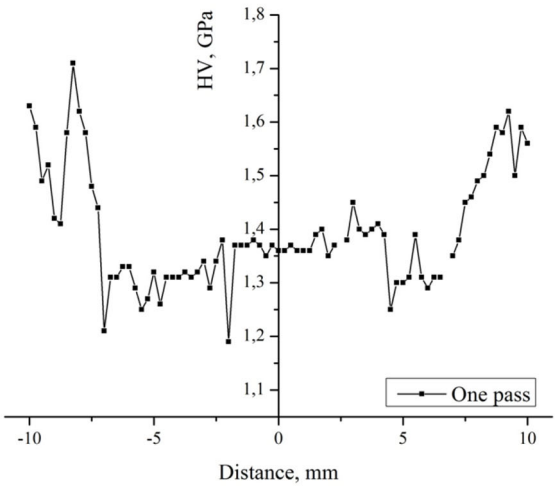

b)

Fig. 3 The single-pass (sample 1) FSP macrostructure (**a**) and microhardness profile (**b**) on an AA2024 sample

3.1.2 Two-pass FSP

A two-pass FSPed sample (Fig. 6a) shows all the above-described zones as well as an extra TMAz and a joint line formed in the overlap zone between two successively made tracks (Fig. 7a). The minimum microhardness was measured in the TMAZ and HAZ on the retreating side of the track (Fig. 6b). Somewhat higher microhardness was detected in the re-heated and re-stirred parts of the SZ1 (***haz 1–2* and *tmaz 1–2*).** The SZ2 metal is characterized by even higher microhardness which then falls at the TMAZ on the advancing side of the track no. 2.

The macroscopic joint line between stirring zone 1 and stirring zone 2 is analogous to that formed between the stirring zone 1 and the TMAZ I (Fig. 7b).

3.1.3 Three-pass FSP

Even more the clearly the joint line is observed in a three-pass FSP sample between stir zone II and stir zone III (retreating

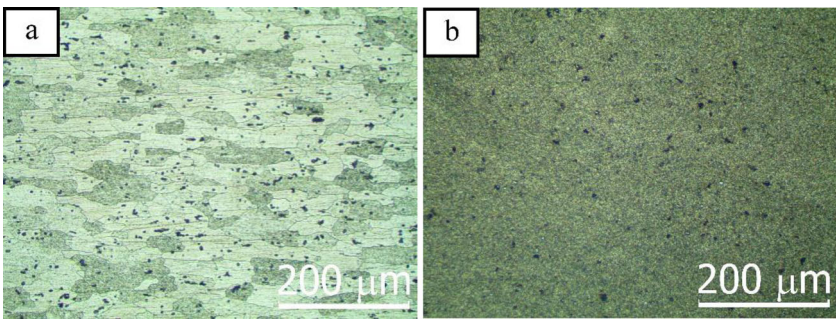

Fig. 4 The microstructures of the base AA2024 metal (**a**) and stirring zone I (**b**)

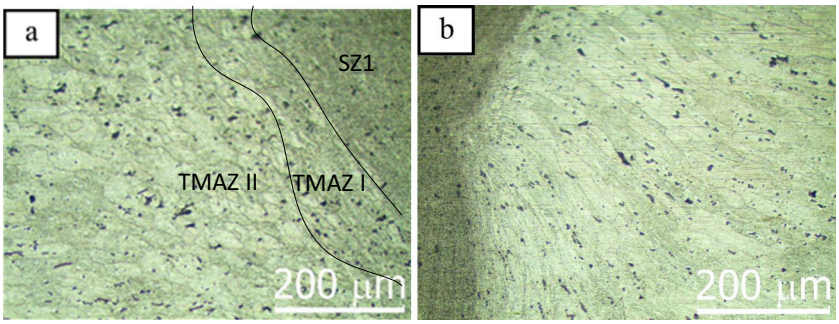

Fig. 5 The microstructures of retreating side (**a**) and advancing side (**b**) TMAZ in a single-pass FSP metal

side ***tmaz 2–3***) (Fig. 8a, pos.4). The microhardness profile shows again the minimum hardness in the TMAZ on the advancing side of track 1 (Fig. 8b) which then gradually grows along the direction SZ1 → SZ2 → SZ3. The SZ1 and SZ2 on the retreating side were subjected to double and single reheating and re-stirring, respectively. The result is that the low hardness region extended as compared with that of the two-pass FSP. It is interesting that the newly formed SZ1/SZ2 ***tmaz 1–2***, and SZ2/SZ3 ***tmaz 2–3*** (Fig. 9a, b) have not revealed any microhardness minimums as those found on the TMAZ. The rationale may be that re-stirred zones and ***tmazs*** were formed in the fine crystalline SZ metal while TMAZs were formed in the coarse-grained base metal.

3.2 Microstructure

The microstructure of one-pass or two-pass stir zones on the advancing side of the seam is characterized by the presence of numerous faced and rod-like particles. Many of them are localized on the grain boundaries. The grain boundary migration in recrystallization is pinned by these coarse particles (indicated by arrows in Fig. 10a). Also one can see screw dislocations pinned by smaller particles inside the grain bodies (see arrows in Fig. 10b) which may be the result of dragging the particles by the migrating boundary.

The TEM images show that these coarse particles are stable non-coherent Al_2CuMg and dispersoids (Fig. 11 c, d–f). The grain size distribution is shown in Fig. 12a from where it follows that the mean size of solid solution grains is 1.12 ± 0.34 μm.

The microstructure of SZ2 is composed of the same S-phase particles and dispersoids as that of SZ1 but it seems that they precipitate from the solid solution in more quantities as compared with SZ1 zone (Fig. 13a). Also, more dislocations are noticed in this area (Fig. 13b). Such a difference might be explained by more heat released from friction on this side as

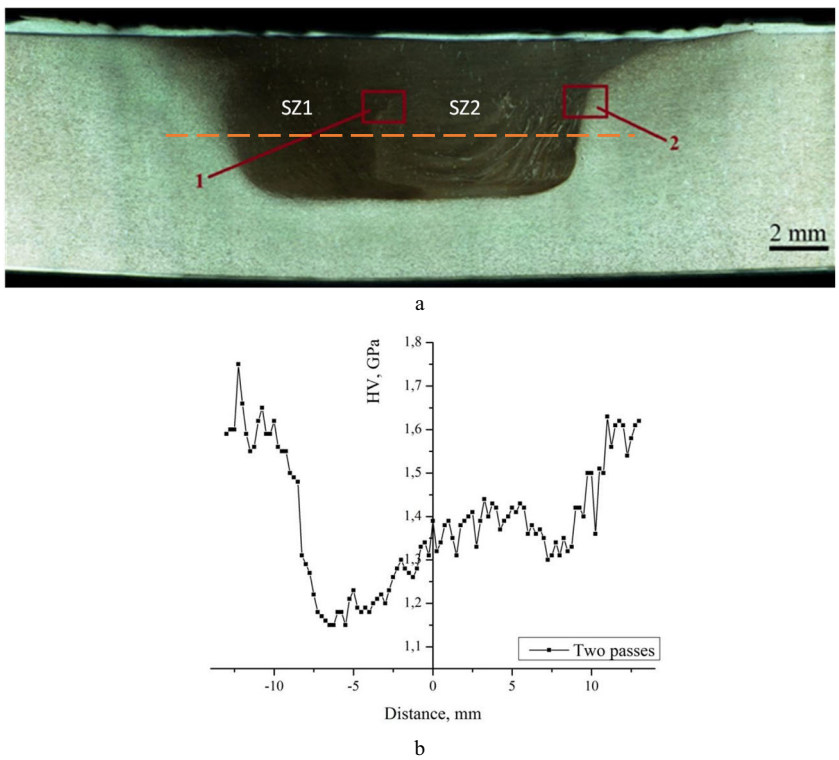

Fig. 6 The double-pass (sample 2) FSP macrostructure (**a**) and microhardness profile (**b**) on an AA2024 sample

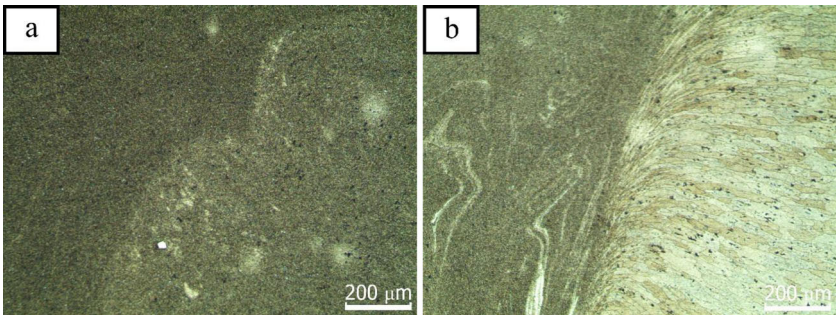

Fig. 7 The joint lines between stirring zone 1 and re-stirred zone II TMAZ (**a**) and between the re-stirred zone II and advancing side TMAZ (**b**)

compared with that on the RS and therefore more S(S′) phase precipitated. The smallest particles may be related to semi-coherent S′ and GPB particles.

The microstructure of the TMAZ II is shown in Fig. 14 where one can see the effect of extra aging from re-heating in the form of numerous S(S′) particles (Fig. 14b). The SAED microdiffraction pattern in Fig. 14c allows identifying the S-phase reflections $(021)_S$, $(023)_S$ and $(06\overline{4})_S$ that allow observing both large and fine S-precipitates (Fig. 14c, d–f).

The volume content and mean size of the of S(S′)—precipitates in the SZ2 advancing side were 3.95 ± 1.14 vol.% and 11 ± 5 nm as compared with 2.49 ± 0.27 vol.% and 32 ± 10 nm on the SZ1 retreating side. One may suggest therefore that re-heating caused the S(S′)—precipitates growth and over-aging which is in accordance with the lower microhardness inherent for this region.

3.3 Tensile tests

Fracture was localized on the retreating side of the FSP track in all three cases (Fig. 15) The ultimate stress of the FSPed samples was at the level of 400 MPa (Fig. 16). The maximum and minimum elongations were demonstrated by one-pass and two-pass FSPed samples, respectively. Also, the two-pass FSPed sample showed the minimum ultimate strength.

4 Discussion

The single-pass FSP on AA 2024 produced a microstructure similar to that obtained after FSW butt joining two plate workpieces. It is typical that the recrystallized grains in the stirring zone have different sizes because of the Zener pinning the

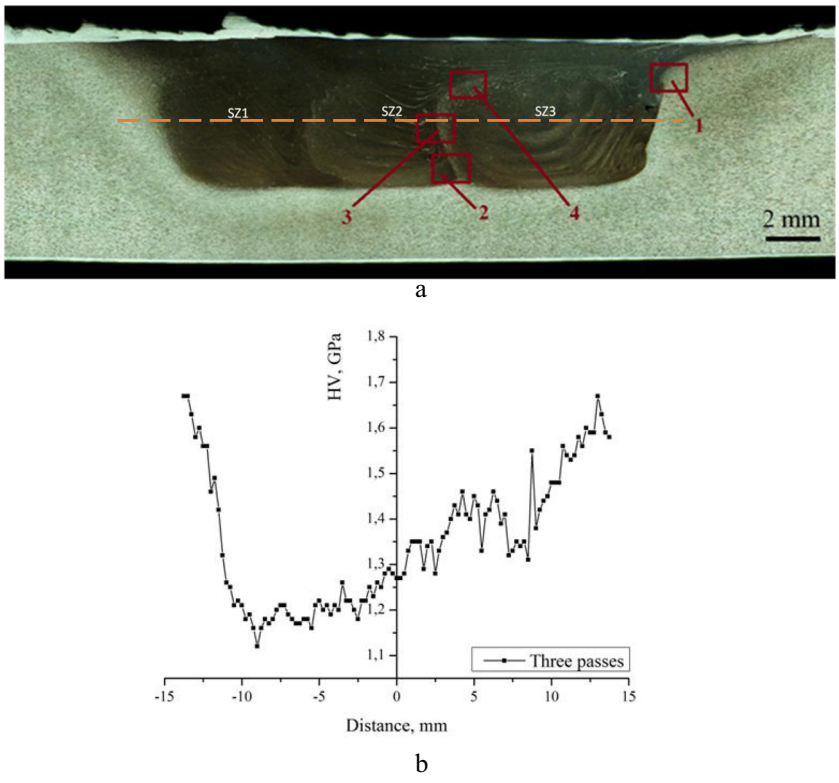

Fig. 8 The macrostructure (**a**) and microhardness (**b**) of the three-pass (sample 3) FSP metal

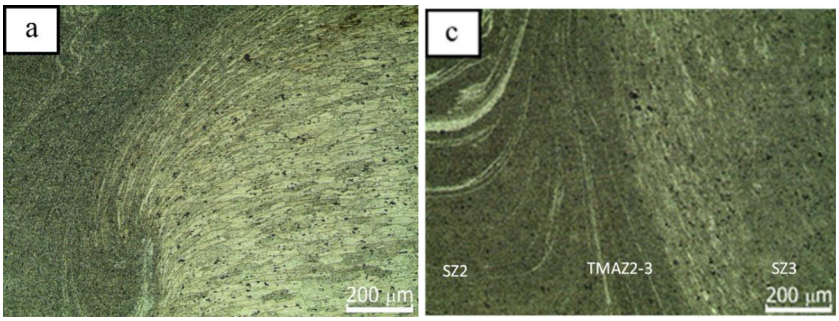

Fig. 9 The joint line between stirring zone 2 and re-stirred zone 3 TMAZ (**a**) and ***tmaz 2–3*** zone between SZ2 and SZ3 (**b**)

migrating boundaries on the stable coarse precipitates, which precipitated from both hot and plasticized metal before final recrystallization stage has begun. In fact, accelerated diffusion in the superplastic ultrafine-grained hot material was so fast that solid solution decomposed very quickly into an over-aged state with coarse S-phase particles and low hardness.

The preliminary assumption necessary for such a fast aging is that all particles both soluble and insoluble ones are dissolved in the course of FSP thus creating a supersaturated solution. Such an assumption is verified by the fact that many precipitates are faced and therefore cannot be the fragments of initial insoluble particles. Also, this suggestion is supported by dos Santos et al. [7, 8] who observed it on aluminum alloys using a small angle X-ray scattering. Therefore, the first stage of the FSW will be deformation dissolution of the initially present insoluble particles and formation of re-saturated solid solution. When a portion of this plasticized solid solution is carried to the rear zone behind the tool and it sticks then to the previously deposited one, there immediately starts precipitation of particles and recrystallization of grains. It seems that particles precipitate first since the recrystallizing grain boundary is pinned by them or drags them. According to Rollett et al. [9] Zener pinning is of high importance in retarding the primary recrystallization. However, it was shown by Fu et al. [10] that average hardness showed a strong dependence on the rotation rate and therefore the stirring zone metal still has a potential for further aging at higher temperatures achieved by increasing the process heat input.

When analyzing the microhardness profiles of the samples, one can see that the microhardness is slowly growing across the stirring zone (zones) from its retreating side to advancing. Such a tendency might be the result of extra aging of the metal due to heat input inhomogeneity. Hersent et al. [11] state that heat production on the advancing side is greater and a thermal cycle is not symmetrical with respect to the FSP seam. Therefore, the advancing side metal has more potential for extra aging and increasing hardness. Such an assumption is supported by observation of very fine precipitates on the advancing side of stirring zone 2 (Fig. 13b) which could be the result of such a inhomogeneous heat distribution.

It is known that TMAZ may be divided into thin fine crystalline TMAZ I adjacent to the SZ and coarse-grained TMAZ II adjacent to the HAZ. The SZ metal flows are being driven by the FSW tool pin against the base metal thus creating a sliding friction experiment conditions when the subsurface metal is severely deformed and dragged thus forming a high-strain gradient subsurface layer (IIIa or TMAZ I) and plastic strain zone III (TMAZ I+TMAZ II) (Fig. 17). Such an analogy allows a better understanding of the microstructural evolution of the metal from the standpoint of tribology.

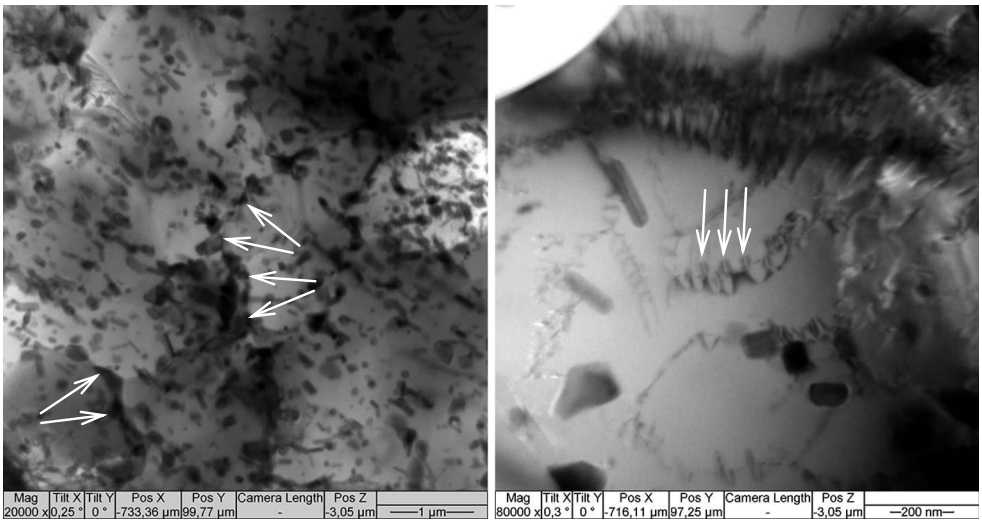

Fig. 10 The light field TEM images of 1-pass FSPed stirring zone microstructures

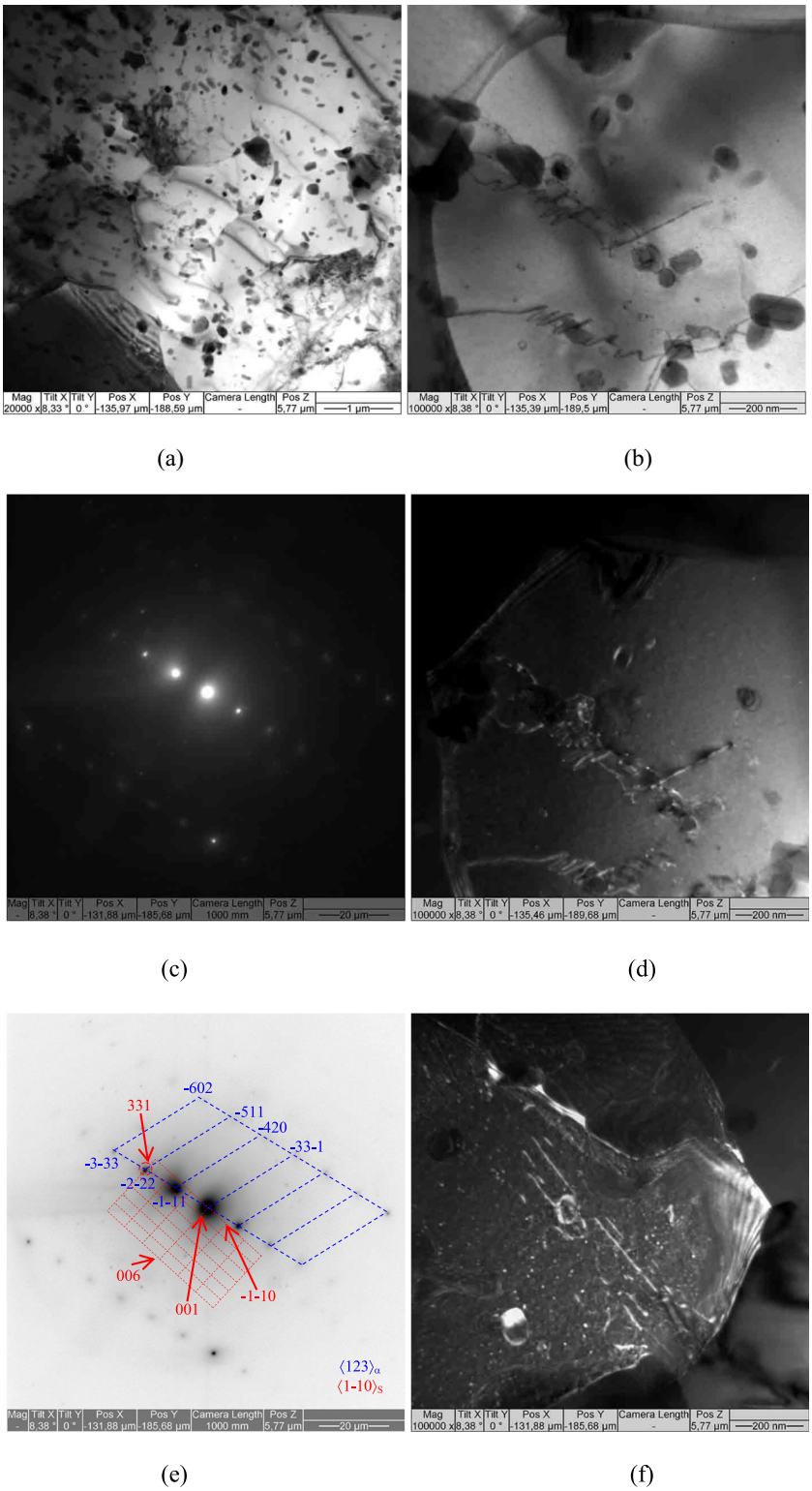

Fig. 11 The TEM bright-field (**a**, **b**) images and corresponding SAED microdiffraction pattern of stirring zone 1 (SZ1) re-heated by two-pass FSP 2 (c). The dark-field images (**d**, **e**, **f**) have been obtained using $(\overline{2}\overline{2}2)_{\alpha}$ and $(331)_{S}$, reflections in Fig. 10c

Both normal load and friction forces act on the interface between the SZ metal flow and TMAZ I. The TMAZ strain rate is less than that of the SZ metal and it only accumulates strain when SZ experiences also a dynamic recrystallization. Friction between the SZ and TMAZ metals generates extra heat thus increasing the layer temperature and thermal softening. The strain is increased so that TMAZ I generates fine or even nanocrystalline thin layer. However, this layer may adhere to the SZ metal and flow at a high rate or may deform plastically at a low flow rate. This is what happens during

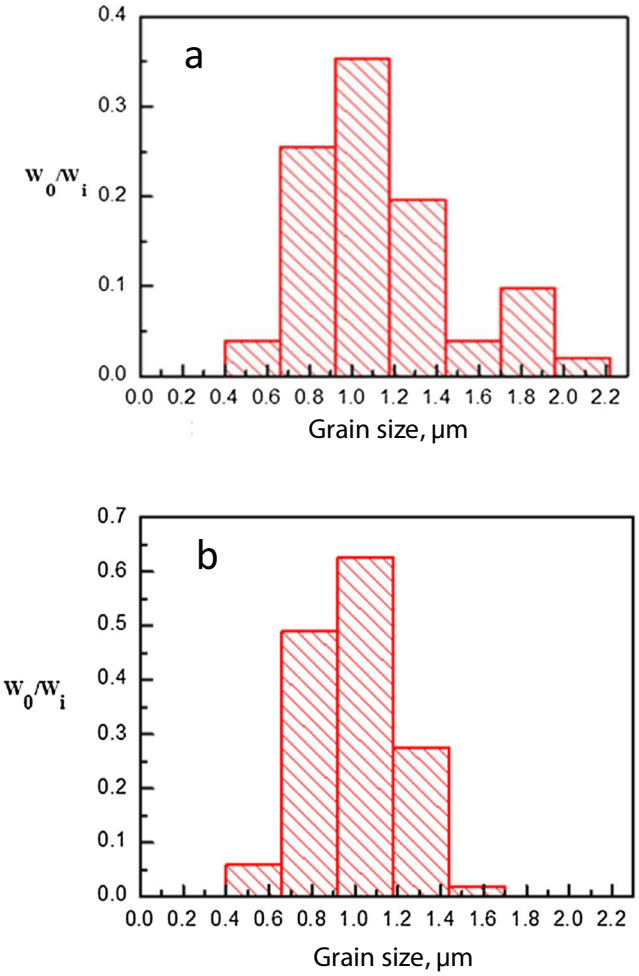

Fig. 12 Grain size distribution in the re-heated part of SZ1 after two-pass FSP (**a**) and in the SZ2 on the advancing side of the seam (**b**). Mean grain size is 1.12 ± 0.34 μm and 0.96 ± 0.25 μm, respectively

unlubricated sliding experiments on soft metals. The same may be true for the friction stir welding.

In case of multipass friction stir processing, the tool is introduced into recrystallized and fine-grained SZ metal formed by a previous track. Therefore, less mechanical energy is spent for grain deformation and refining. The fine-grained metal becomes quickly involved in a FSP tool–driven quasi-viscous flow thus forming a new type TMAZ composed of only fine grains, which deform according to the grain boundary slipping mechanism when strain dissolution and re-precipitation processes are in dynamic equilibrium.

When measuring the microhardness number distribution over the friction stir–welded joint cross section, some authors did not pay much attention to the structural differences between TMAZ I and TMAZ II. However, these differences are important in aging materials such as AA2024 [10].

The strain accumulated in the III (TMAZ II) zone may be evaluated using a simplified version of formula obtained by Dautzenberg and Zaat [12] for determining effective deformation from deflection of the grain boundaries under sliding:

$$\varepsilon = \frac{\sqrt{3}}{3}\tan\Theta \text{ [12]},$$

where Θ is the angle between normal to the worn surface and tangent to the curved grain boundary of (Fig. 16). The strain accumulated in the IIIa layer becomes higher than 100% and cannot be evaluated using the formula. All we know is that the grain size has been reduced by a factor of 50.

Straumal et al. analyzed precipitation and dissolution in Cu-Ag alloys and in severe plastic deformation high-pressure torsion in terms of concurrent precipitation and dissolution processes [13]. Such a suggestion fully fits in a FSW

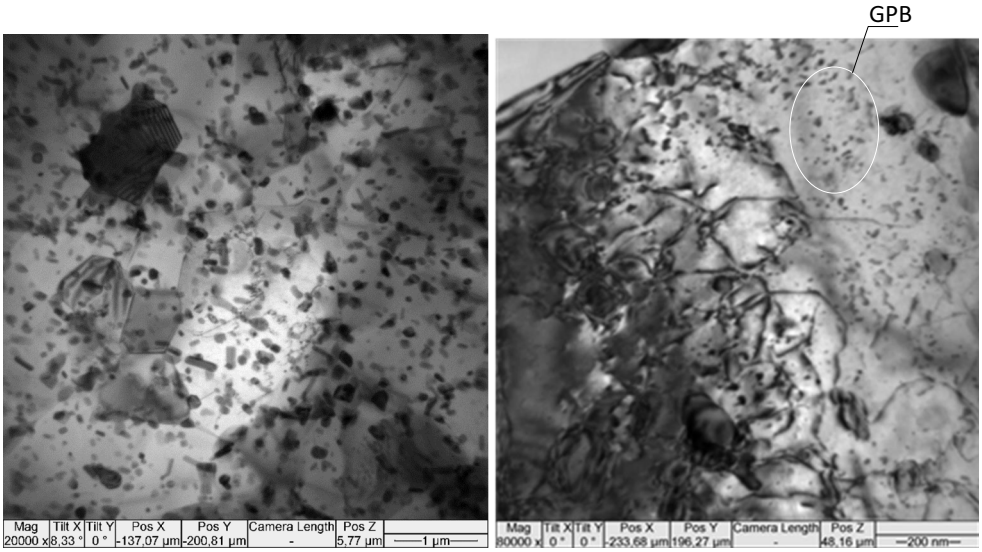

Fig. 13 The TEM images of SZ2/TMAZ I microstructure of the two-pass FSP seam on the advancing side of the seam. Smallest precipitates found in the oval area in Fig. 13b can be related to GPB zones

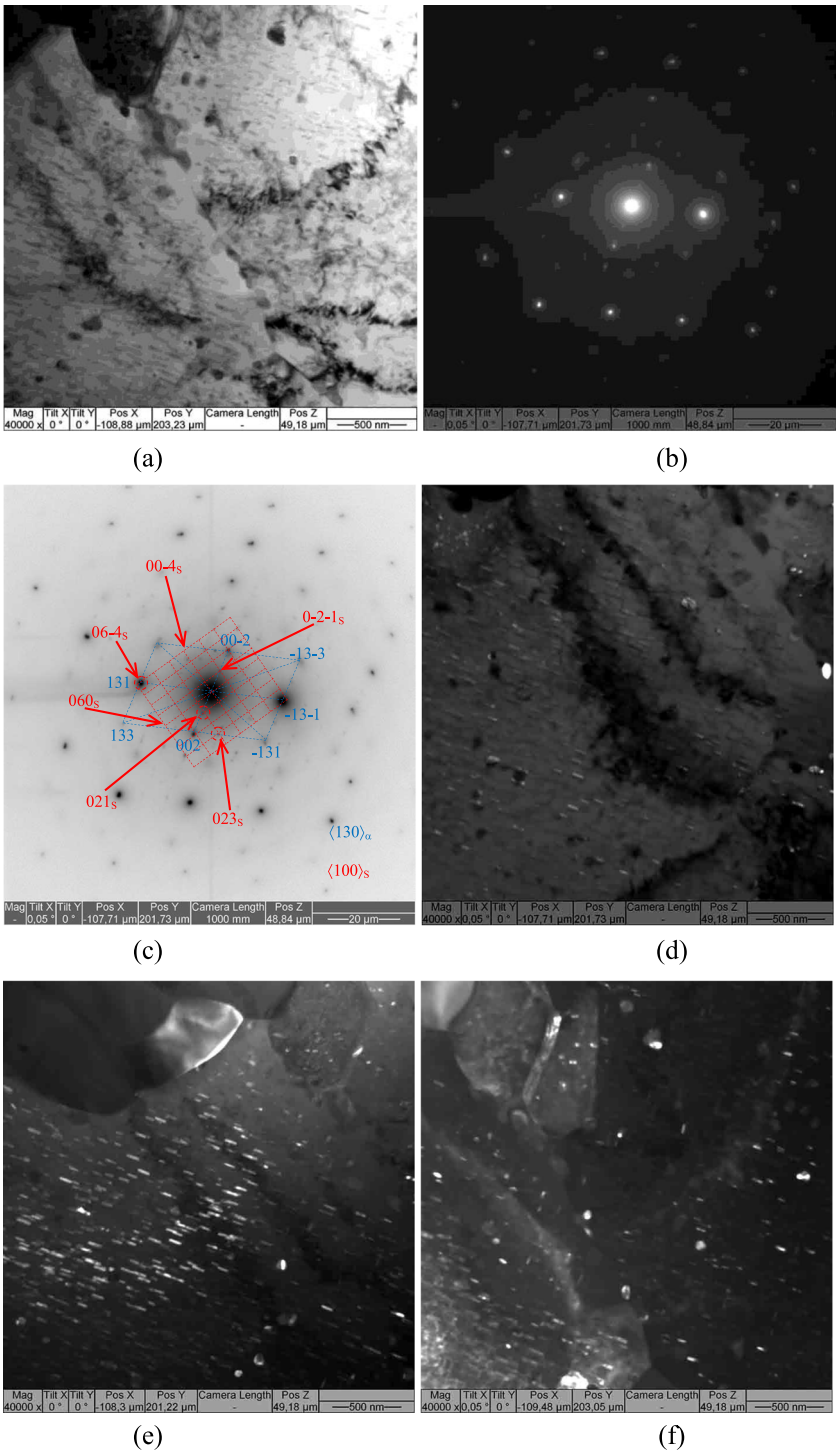

Fig. 14 The bright-field TEM image (**a**) and SAD microdifraction 2 patterns (**b**, **c**) of TMAZ II microstructure on the retreating side of the two-pass FSP seam (**a**, **b**, **c**). The dark-field images (**d**, **e**, **f**) were obtained using $(021)_S$ (**d**), $(023)_S$ (**e**), and $(131)_\alpha$ and $(06\overline{4})_S$ (**f**), reflections

process when initial particles break and dissolve. Further stirring allows homogenizing the solid solution and simultaneously launches its decomposition by precipitation. The two concurrent processes are in dynamic equilibrium during FSW. However, TMAZ/SZ boundary is the surface where flowing SZ metal and immobile TMAZ metal contact each other. In other words, this is a velocity (strain rate) discontinuity surface where quasi-viscous SZ metal slows down thus forming a boundary layer. Also, since the SZ metal slides over the TMAZ metal, this surface will serve as an extra heat source. Therefore, decomposition will dominate here over the dissolution and large precipitates may grow here. The solid solution will be depleted by the alloying elements and no further hardening precipitation will be possible. The precipitation-free zones around large coagulating precipitates may be the result of such a depleting process.

Fig. 15 Fracture localization on the retreating side of the FSP track

The plasticized SZ metal flows being driven by the FSW tool and the above-discussed dynamic equilibrium is supported until the moment when it finally sticks to the previously deposited layer [14]. The deformation dissolution stops here and precipitation is in full force thus creating an over-aged and recrystallized microstructure shown in Fig. 10.

The TMAZ I layer is an over-aged zone as compared with both SZ and HAZ; therefore, its microhardness and strength are minimum values there. Thus over-aged TMAZ I gives minimum hardness zones which do not disappear even after extra-natural or artificial aging.

At the same time, the TMAZ metal is subjected to plastic deformation and adhesion from the flowing SZ metal so that a nanocrystalline subsurface layer may be generated in it which is capable of a quasi-viscous flow. Analogous phenomena occur in sliding tests on ductile metals when sliding-generated nanocrystalline layer flows over deformed base metal according to grain boundary slipping [15]. This layer forms a nanosized grain layer known as TMAZ I after cooling. When analyzing the role played by adhesion in FSW weld formation, it was suggested [14] that such a metal layer may stick either to FSW tool or the SZ flowing metal and thus create a new velocity discontinuity surface and extra heat generation.

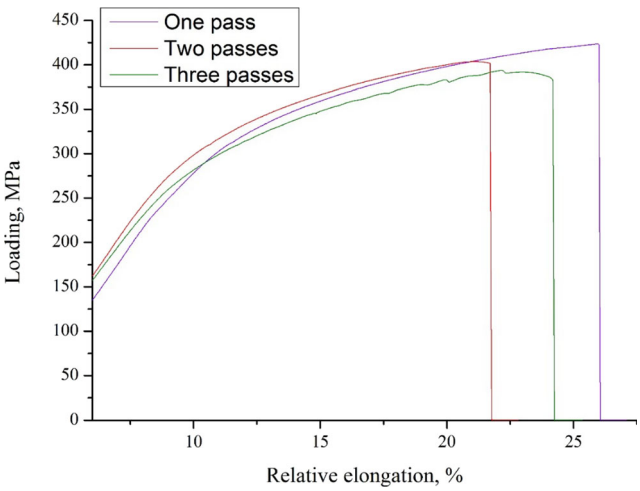

Fig. 16 Tensile load/elongation diagrams for the FSPed samples

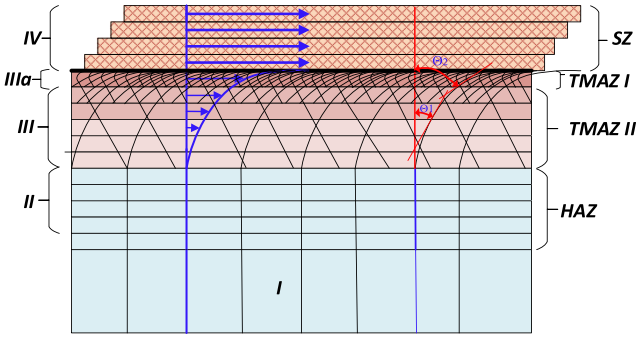

Fig. 17 Schematics of zones formed in sliding friction and friction stir welding. I—base metal; II—elastic strain zone or HAZ; III—plastic strain zone or TMAZ; IIIa—high-strain gradient layer or TMAZ I, and IV—quasi-viscous nanocrystalline layer flow or SZ

In our opinion, such a suggestion serves to better understand the layered macrostructure of the FSW weld, which is obtained even in the case of using a not-threaded tool. As concluded by Lorrain et al., an unthreaded tool provides the plasticized metal flow similar to that produced by a threaded one [16]. While being transferred to the cohesion zone, this layer slides over the less deformed base metal thus generating friction heat and bringing it closer to the advancing side where this layer is detached from the tool, sticks to the previously deposited layer, and is finally recrystallized. It is possible that this extra heat facilitates precipitation closer to the advancing side of the weld. The grain growth by recrystallization is retarded here by the precipitates. Therefore, TMAZ I is always a fine crystalline layer.

The extra TMAZs formed between SZ1/SZ2 and SZ2/SZ3 are characterized by easy deformation and adhesion of previously FSPed SZ1 and SZ2 metals, respectively. In this case, there is no such narrow localization of the velocity discontinuity surface since a wider layer of metal is involved in the flow motion together with the new FSP track one. Therefore, it becomes hard to detect any the extra precipitation on these SZ1/SZ2 and SZ2/SZ3 boundary surfaces.

The TMAZ II zone is structurally similar to the HAZ, i.e., consists of coarse non-refined but plastically deformed grains containing both insoluble equilibrium precipitates and lath S(S′) phases which attribute high hardness to this zone. No over-aging occurs in TMAZ II unless heating was high enough.

5 Conclusion

The overlap zones between the MP-FSP tracks are characterized by the presence of clearly seen ***tmaz*** zones formed between the neighboring stirring zones belonging to successively made FSP tracks. These ***tmaz*** reveal their layered macrostructures formed by sliding friction from the stirring zone

metal flows. No differences in microhardness were observed in these zones.

The MP-FSP stirring zones formed in AA2024 are composed of solid solution and coarse S-phase particles, i.e. it is a microstructure inherent to an over-aged state. Such a state is a result of post-stirring precipitation of these particles in the absence of the dissolution effect of stirring.

Even higher over-aging effect is achieved on the boundary between stirring zones and HAZ metal i.e. TMAZ I, where precipitation always dominated over the strain dissolution. The fine crystalline TMAZ I formation is caused by deformation of the HAZ metal by the stirred metal flow friction analogous to how it occurs during a sliding test on ductile metals. TMAZ II is located far off the stirring zone and close to HAZ; therefore, metal here is subjected only to precipitation of fine orthogonally oriented S(S′) particles which cause hardening.

The over-aged structure of TMAZ I is responsible for the formation of a weak zone and tensile fracture localization on the retreating side of the tracks.

The necessity of distinguishing between TMAZ I and TMAZ II stems from the results of experiments found in literature when whole TMAZ is referred to as an over-aged zone but its TEM images show the abundance of orthogonal S(S′) precipitates which are inherent only to HAZ and TMAZ II which are not over-aged.

Acknowledgments This study was performed within the frame of the Fundamental Research Program of the State Academies of Sciences for 2013–2020, line of research III.23.

References

1. Gandra J, Miranda RM, Vilaca P (2011) Effect of overlapping direction in multipass friction stir processing. Mater Sci Eng A 528: 5592–5599
2. Gnyusov SF, Degterev AS, Tarasov SY (2018) The effect of plasma torch weaving on microstructural evolution in multiple-pass plasma-transferred arc Fe-Cr-V-Mo-C coating. Surf Coat Technol 344: 75–84
3. Kalashnikova TA, Chumaevskii AV, Rubtsov VE, Tarasov SY, Ivanov AN, Alibatyrov AA, Kalashnikov KN (2017) AA2024 microstructural evolution after bidirectional friction stir processing. AIP Conf Proc 1909:020078-1-020078-4. https://doi.org/10.1063/1.5013759
4. Brown R, Tang W, Reynolds AP (2009) Multi-pass friction stir welding in alloy 7050-T7451: effects on weld response variables and on weld properties. Mater Sci Eng A 513–514:115–121
5. Genevois C, Fabregue D, Deschamps A, Poole WJ (2006) On the coupling between precipitation and plastic deformation in relation with friction stir welding of AA2024 T3 aluminium alloy. Mater Sci Eng A 441:39–48
6. Abraham F (2012) Tensile properties and fracture behavior of Multipass Friction Stir Processed Al-7Si-0.3 Mg cast alloy. A thesis submitted in partial fulfillment of the degree of Master of Engineering., AUT University, Auckland, New Zealand
7. dos Santos JF, Staron P, Fischer T, Robson JD, Kostka A, Colegrove P, Wang H, Hilgert J, Bergmann L, Hütsch LL, Huber N, Schreyer A (2018) Understanding precipitate evolution during friction stir welding of Al-Zn-Mg-Cu alloy through in-situ measurement coupled with simulation. Acta Mater 148:163–172. https://doi.org/10.1016/j.actamat.2018.01.020
8. Nascimento F, Santos T, Vilac P¸ Miranda RM, Quintino L (2009) Mater Sci Eng A 506:16–22
9. Rollett A, Humphreys F, Rohrer GS, Hatherly M (2004) Recrystallization and related annealing phenomena, 2nd edn. Pergammon 658p. (p304)
10. Fu R, Zhang J, Li Y, Kang J, Liu H, Zhang F (2013) Effect of welding heat input and post-welding natural aging on hardness of stir zone for friction stir-welded 2024-T3 aluminum alloy thin-sheet. Mater Sci Eng A 559:319–324
11. Hersent E, Driver JH, Piot D, Desrayaud C (2010) Integrated modelling of precipitation during friction stir welding of 2024-T3 aluminum alloy. Mater Sci Technol 26(11):1345–1352. https://doi.org/10.1179/026708310X12798718274511
12. Dautzenberg JH, Zaat JH (1973) Quantitative determination of deformation by sliding wear. Wear 23(1):9–19
13. Straumal BB, Pontikis V, Kilmametov AR, Mazilkin AA, Dobatkin, Baretzky B (2017) Competition between precipitation and dissolution in Cu-Ag alloys under high pressure torsion. Acta Mater 122:60–71. https://doi.org/10.1016/j.actamat.2016.09.024
14. Tarasov SY, Filippov AV, Kolubaev EA, Kalashnikova TA (2017) Adhesion transfer in sliding a steel ball against an aluminum alloy. Tribol Int 115:191–198. https://doi.org/10.1016/j.triboint.2017.05.039
15. Tarasov SY, Rubtsov VE (2011) Shear instability in the subsurface layer of a material in friction. Phys Solid State 53(2):358–362
16. Lorrain O, Favier V, Zahrouni H, Lawrjaniec D (2010) Understanding the material flow path of friction stir welding process using unthreaded tools. J Mater Proc Technol 210:603–609. https://doi.org/10.1016/j.jmatprotec.2009.11.005